The effect of clay surface charge on the emerging properties of Polystyrene-organoclay nanocomposites

Henrik Mauroy*[a,b], Tomás S. Plivelic[c] ,Elisabeth L. Hansen[d], Jon Otto Fossum[d], Geir Helgesen[a,b] and Kenneth D. Knudsen*[a,d]

[a]Physics department, Institute for Energy Technology, P.O. Box 40, N-2027 Kjeller, Norway

[b]Department of Physics, University of Oslo, N-0316 Oslo, Norway

[c]MAX IV Laboratory, Lund University, P.O. Box 118, SE-221 00 Lund, Sweden

[d]Department of Physics, Norwegian University of Science and Technology, Hoegskoleringen 5, N-7491 Trondheim, Norway

*E-mail: Kenneth D. Knudsen: kenneth.knudsen@ife.no; Henrik Mauroy: henrik.mauroy@ife.no

Polystyrene-organoclay nanocomposites, wide angle x-ray scattering, clay, cation exchange capacity (CEC)

A series of polystyrene-clay nanocomposites, based on two natural clay types (Na-Montmorillonite and Hectorite), and two synthetic clays (Laponite and Li-Fluorohectorite), were prepared via in situ intercalative polymerization after surface modification with an organic

1

ammonium cation (CTAB). The structural characteristics of the organically modified clays as well as the nanocomposites were investigated by means of wide angle x-ray scattering (WAXS), and the thermal properties were studied with TGA. In organically modified clays, the silicate interlayer spacing increases and the magnitude seems to be directly correlated with the amount of clay surface charge. In nanocomposites, polymer intercalation is also observed but partial exfoliation is present, modifying significantly the morphology of the material. The degree of dispersion of the clay platelets, as well as the resulting properties of the nanocomposites, were found again to be systematically, and almost linearly correlated with the intrinsic surface charge of the clays, which varied between 44 and 120 meq/100g. Increased dispersion was seen in the nanocomposites made from clays with low surface charge, here Hectorite and Laponite, suggesting that these can be suitable alternatives to the more employed Montmorillonite for enhancement of thermal properties. The thermal stability was found to be better for the nanocomposites than for the pure polystyrene.

1 Introduction

In polymer materials science a promising class of high-performance composite materials has been explored during recent years. By combining polymer systems with miniature particles, where at least one of the particle dimensions is in the nanometer range, remarkable modifications in material properties can be achieved. Such polymer nanocomposite materials exhibit improved flame retarding properties[1,2] and mechanical performance[3,4] compared to the pristine polymers. In some nanocomposites, less than one weight percent of nanoparticle filler can drastically modify the overall macroscopic system behavior, provided that the incorporated particles are well-dispersed and their surface can interact sufficiently with the polymer chains.[5] For the enhancement of mechanical properties anisometric filler particles are preferred, especially

40   lamellar types such as exfoliated clay, because the reinforcing effect is strongly related to the

41   aspect ratio (diameter to thickness) of the particles.[6]

42   In the late 1980s Toyota Motor Company invented a new type of polymer composite[7,8] made

43   by polymerizing ε-caprolactam in the presence of a few weight percent of organically surface

44   treated montmorillonite (MMT) to create a nylon 6-clay nanocomposite with fully exfoliated

45   clay platelets inside the polymer matrix. This material demonstrated superior thermal and

46   mechanical properties compared to conventional nylon 6 composites, due to the intimate mixing

47   of nanometer sized clay particles and polymer chains, and it was quickly utilized in one of their

48   production cars.[8]

49   Since then many industrially important polymer systems have been explored, such as

50   polypropylene (PP)[9] and polystyrene (PS).[10] PS-clay systems are of interest to employ as model

51   compounds, not only because of the widespread use of PS in connection with engineering and

52   commercial products, but also because of the amorphous nature of this polymer. Any changes in

53   overall properties will then be due mainly to the additives used. One major complication with PS

54   is that it is hydrophobic and not miscible with clay, making exfoliation and dispersion of the clay

55   particles difficult.[11] The workaround is to render the clay hydrophobic by exchanging the

56   intercalated cations with organic chain molecules, such as alkyl ammonium ions or fatty acids,

57   through a simple cation exchange process.[6] Since the early work on PS-clay by Vaia et al.,[12]

58   extensive studies have been carried out to synthesize and produce compatible PS-clay systems,

59   where the most used techniques involve melt compounding of the neat polymer with surface

60   treated clays, and *in situ* intercalative polymerization.[13]

61   The latter process can disperse the clay platelets to a larger extent.[11] This technique involves

62   adding clay to the liquid styrene monomer followed by polymerization. The intimate mixing

63   prior to polymerization intercalates styrene molecules into the clay galleries, resulting in a

64   swelled clay structure more susceptible to exfoliation. The degree of further swelling and

65   intercalation of PS-chains are governed by the miscibility between the clay surface and PS. For

66   example, Hasegawa et al.[10] managed to prepare fully exfoliated PS-MMT nanocomposites by

67   using PS co-polymerized with polar oxazoline groups. Fu et al.[14] and Zhu et al.[15] on the other

68   hand, used surfactants with reactive vinyl groups attached to reach a similar and fully exfoliated

69   PS-MMT structure.

70   The clay mostly used for polymer reinforcement is of the 2:1 type where an octahedral metal-

71   hydroxide sheet is sandwiched between two tetrahedral silicate-sheets sharing apical oxygen

72   atoms. Due to isomorphous substitution in to the clay structure, of Si^{4+}, Mg^{2+} or Al^{3+} by cations

73   with a lower charge, a net negative surface charge is formed on each clay platelet. This charge is

74   balanced by exchangeable cations such as Li^+, Na^+ and Ca^{2+} which are shared between adjacent

75   clay platelets.[16] This arrangement leads to a property called cation exchange capacity (CEC),

76   which varies between different 2:1 clays, and is therefore an important intrinsic property of the

77   clays.

78   To the best of our knowledge, the range of clay types used in earlier works on PS-clay

79   nanocomposites, prepared with *in situ* intercalative polymerization, is narrow. There is an

80   extensive use of MMT clay[11], but only a few reports using other clays.[1,17-20] In the present work

81   we have therefore aimed to explore in a systematic manner the differences between several 2:1

82   clays, and to investigate the significance of the effect that the CEC has on the emerging

83   properties of the nanocomposites. Four different types of clay, Hectorite (HT), Laponite (Lp), Li-

84   Fluorohectorite (Fh), as well as MMT were chosen based on their large span in CEC values.

2 Experimental

2.1 Materials

Styrene monomer (≥99%), Benzoyl peroxide (Luperox® A75, 25 % water) and cetyltrimethylammonium bromide (CTAB) (≥98%) were purchased from Sigma-Aldrich and used without further purification. Two synthetic 2:1 clays, Laponite XLG (Lp) and Li-Fluorohectorite (Fh), were kindly donated by Andreas Jennow AB, and purchased from Corning Inc, respectively. Two natural 2:1 clays, Na-Montmorillonite SWy-2 (MMT) and Hectorite SHCa-1 (HT), were purchased from The Clay Minerals Society Repository. These four clays share the same 2:1 phyllosilicate structure. The type of exchangeable cations and the CEC-values of the clays used here and reported by the manufacturers are listed in Table 1.

The lateral size of Fh platelets is large[1] and is during the synthesis in this work limited to ~1 µm by centrifugation, while Lp platelets have a much smaller, and fairly narrow, size distribution centred around 30 nm.[21] MMT and HT platelets lie in between these two extremes, at 0.1-1 µm and 0.1-0.4 µm, respectively.[1,22,23]

Table 1. Experimental details of the clays and the amount of CTAB added to the clay.

Clay type	Exchangeable cation[†]	CEC (meq/100g)[†]
HT	Na, Mg	44
Lp	Na	47
MMT	Ca,Na	77
Fh	Li	120

[†] HT, MMT see ref. [24], Lp, Fh see ref. [16]

2.2 Preparation/synthesis

2.2.1 Organoclays

The clays were surface modified using CTAB through a simple cation-exchange process, where the ammonium cation of CTAB replaces the inorganic cations between the clay platelets. In the present work the amount of CTAB used corresponded to four times the cation exchange capacity (CEC) of the respective clay. The clays were first crushed in a mortar, dispersed in deionized water and stirred at 80 °C for 12 hours in order to exfoliate the clay platelets. Subsequently the suspensions were cooled down and centrifuged at 700G (maximum speed) for 25 minutes to remove non-clay constituents that were present in the natural clays. This treatment also removed clay particles larger than ~1 μm.[25] After centrifugation, the supernatant contained a stable semi-transparent dispersion of exfoliated clay that did not sediment, and the concentration of clay was determined by evaporating a known volume and weighing the solid residue. Since Laponite undergoes a near complete exfoliation by dispersion in water at room temperature, centrifugation was omitted and the suspension was only stirred at 80 °C for 2 hours.

A predefined amount of CTAB, corresponding to 4×CEC (surplus of surfactant) of each clay, was dissolved in deionized water at 30 °C until the solution turned clear. Subsequently the clay suspensions were heated to 80 °C, and the CTAB-solution was poured gently in under stirring. Flocks of hydrophobic surface modified clay precipitated immediately. The solutions were then stirred at 80 °C for 12 hours, and subsequently left at room temperature for 24 hours to settle. The solutions were decanted and suction filtrated, and the precipitate was washed with 100 mL deionized water, stirred for 1 hour and suction filtrated again. Washing and filtration was repeated up to 10 times to remove any residual CTAB. After each wash cycle the waste solutions were checked for Br-ions (free CTAB molecules) by adding some drops of 0.5 M AgNO$_3$. After the last filtration, the filtrate was dried in an oven at 80 °C overnight, crushed to a fine powder in

125   a mortar, and stored in a sealed container until further studies. The organoclays were labelled

126   org-HT, org-Lp, org-MMT and org-Fh respectively.

2.2.2 Polystyrene nanocomposites

128   The nanocomposites were prepared with *in situ* free radical polymerization of PS, by the

129   following procedure: In a 2 mL glass bottle a certain amount of organoclay, normalized to 0.03 g

130   of the inorganic part of the clay, was dispersed together with 7 mg initiator (Benzoyl peroxide) in

131   1 mL of styrene monomer. This amounts to 3.2 wt.% of inorganic filler, or roughly 5 wt.% of

132   total organoclay filler (including the surfactant). Pure PS samples were made with the same ratio

133   of monomer to initiator, but without any filler. The solution was vigorously stirred for 2 hours at

134   room temperature, and then for 12 hours at a much lower intensity. Afterwards it was filled in 80

135   mm long square-shaped glass capillaries with inner dimensions of 1.0 mm.

136   Subsequently the open end was connected to a water jet pump, to remove air, and sealed with a

137   flame torch. Immediately after sealing, the samples were immersed in a silicone oil bath, which

138   was kept at 95 °C, and left to polymerize for 5 days.

139   The polymerized nanocomposites were carefully pulled out from the capillaries and labelled

140   PSHT, PSLp, PSMMT and PSFh, respectively. They were studied with wide angle x-ray

141   scattering, optical and electron microscopy, and thermogravimetric analysis. Visual inspection of

142   the samples showed that they were all, except PSFh, semi-transparent with a homogenous white

143   coloring from the clay (see Figure S1 in the supporting information).

2.3 Characterization

2.3.1 Wide angle x-ray scattering (WAXS)

146   WAXS experiments were performed at beamline I911-4 of the MAX-lab synchrotron facility

147   in Lund, Sweden.[26] All data were collected at a wavelength of $\lambda = 0.91$ Å, covering the *q*-range

148   between 0.1 to 10 nm^{-1} ($q=(4\pi/\lambda)\ sin(\theta)$ with *2θ* the scattering angle). The detector used was a

149   two-dimensional CCD (165 mm diameter from MarResearch, Inc). *In situ* heating experiments

150   on the nanocomposites were performed using a customized high temperature furnace (Linkam

151   TS1500) for x-ray scattering experiments. These samples were kept inside the capillaries used

152   for polymerization, and heated from 25 to 250 °C at a rate of 10 °C/min.

153   WAXS-scans of the pure clays were carried out using a NanoSTAR system from Bruker AXS,

154   equipped with a CuKα Xenocs micro source with a wavelength of 1.5418 Å, and a two-

155   dimensional multiwire grid "Xe" gas detector. The exposure times varied from 10 to 20 seconds

156   for the synchrotron experiments, to 60 minutes for the NanoSTAR experiments.

157   Data treatment was performed using the software FIT2D [27] and custom Matlab routines. The

158   synchrotron data were normalized with respect to the transmitted intensity using a photodiode

159   located inside the beam-stop and corrected with respect to the contribution from background

160   scattering.

161   The instrumental peak broadening, used for peak fitting, was determined by measuring the 111

162   reflection from silicon powder.

163   ### 2.3.2   Thermogravimetric analysis (TGA)

164   TGA was performed on a Netsch STA 449 F3 Jupiter TGA-DSC instrument under an argon

165   atmosphere at a heating rate of 10 °C/min from 25 to 650 °C. Other instrumental parameters

166   were adjusted with the software package STA 449F3. A 70 μL alumina crucible was used to hold

167   the samples, which weighed 2-5 mg for the nanocomposites and pure PS, and 15-25 mg for the

168   organoclays. The org-clays were pre-dried prior to measurements to eliminate the signal from

169   absorbed atmospheric moisture.

2.3.3 Transmission electron microscopy (TEM)

TEM imaging of the PSLp and PSHT samples was performed using a JEOL JEM-2000FX transmission electron microscope operated at 200kV. Samples were prepared by placing microtome sections of the composite onto a holey carbon TEM grid.

3 Results and discussion

3.1 Analysis of organoclays

3.1.1 WAXS

In order to verify that the surface modification of the clays was successful, they were measured by WAXS prior to and after modification. The WAXS-curves shown in Figure 1 were used to calculate the average basal spacing between the silicate layers, $d_{001} = 2\pi/q_1$, where q_1 is the q-value at the center of the 001 Bragg-reflection. The basal spacings of the pristine clays were very similar in all cases, varying between 1.1 and 1.3 nm (see Fig 1e). The small variations can be due partly to minor differences in the amounts of intercalated water, since the pristine clays were stored and measured in ambient atmosphere.

On the other hand, there are significant differences in the peak widths (FWHM) of the 001 reflection peak, indicating limited size and/or strain of the silicate layer stacking, depending on the clay type. Pristine Fh presents a very sharp peak whereas the peak from pristine Lp is very broad. This is mainly attributed to the number of clay platelets in each tactoid, being larger in Fh (see also discussion in section 3.2.2). Strain is common in clays and arises due to a large variation in the stacking order of the clay tactoids.[28] Further discussions are presented later.
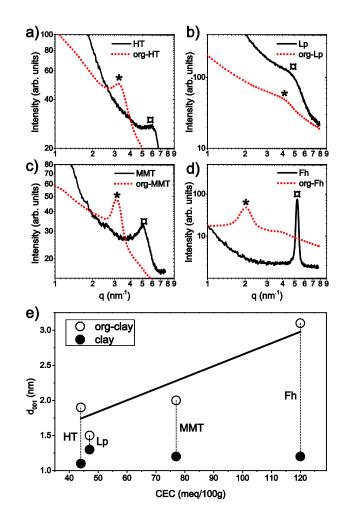
191

Figure 1. (a-d) WAXS-curves of pure clays and organoclays. The 001-reflection is indicated with (¤) and (*) for the pure clays and org-clays, respectively. Curves are scaled arbitrarily to facilitate comparison. (e) The d_{001}-spacing of the clays prior to and after surface modification. The solid line is a guide for the eye.

Table 2. Results from analyzing the organoclays with WAXS and TGA. The different steps of the mass loss are defined in Figure 2. d_{001} values for pure clays are added for comparison.

Clay type	CEC (meq/100g)	Pure clay d_{001}-spacing (nm)	org-clay d_{001}-spacing (nm)	Surfactant mass (%)	Rel. mass loss step 1 (%) (Adsorbed)	Rel. mass loss step 2-3 (%) (Intercalated)

HT	44	1.1	1.9	37	49	51
Lp	47	1.3	1.5	42	36	64
MMT	77	1.2	2.0	41	51	49
Fh	120	1.2	3.1	49	69	31

198

199   After surface modification, the d_{001}-spacing of the organoclays increases due to intercalation of

200   CTAB-cations. The values are shown in Figure 1 and also listed in Table 2. The spacing

201   increases the most for org-Fh, reaching 3.1 nm, while org-MMT and org-HT obtain values of 2.0

202   and 1.9 nm, respectively. Interestingly, this swelling seems to be correlated with the magnitude

203   of the surface charge of the three clays, e.g. Fh has the highest surface charge and hence

204   intercalates more CTAB-cations. However, org-Lp distinguishes itself from the others, showing

205   a very small increase in d_{001}-spacing, although the surface charge of Lp is comparable to HT (see

206   Table 1). A possible cause is that the majority of org-Lp platelets are fully exfoliated when the

207   Lp clay stacks expand above a certain threshold, and therefore do not contribute to the Bragg

208   peak. A peak broadening for all four organically modified clays is also observed, which we

209   interpret as either a reduced number of stacked clay platelets in each tactoid or a sign of uneven

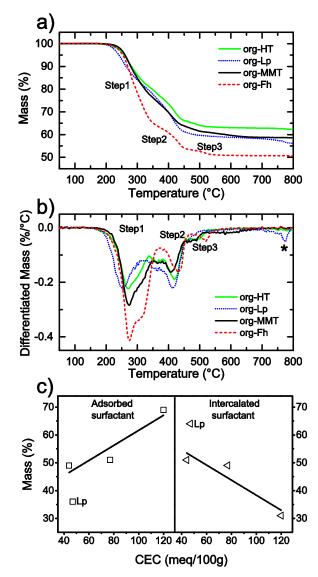210   amounts of intercalated guest molecules from one clay gallery to another.

211   **3.1.2   Thermogravimetric analysis org-clays**

212   Thermogravimetric analysis (TGA) of the organoclays was performed to determine the

213   quantity of surfactant molecules that was intercalated. The results, shown in Figure 2a, and listed

214   in Table 2, indicate a correlation between the uptake of surfactant molecules and the CEC as

215   well. Although CTAB was present in excess (4×CEC), the org-clays with larger surface charge

216   (org-MMT and org-Fh) contained more surfactant, showing an almost linearly correlated

217   increase (see Figure S2 in the supporting information).

218   Furthermore, the TGA-traces indicate that there are three major steps during decomposition of

219   the surfactant.[29] The differentiated TGA-traces (DTGA), shown in Figure 2b, display two peaks

220   above 200 °C for all organoclays. The peaks at around 300 °C are coupled to decomposition step

221   1 which is attributed to a high rate of decomposition of surfactant molecules *adsorbed* on the

222   *outer* surface of the clay particle or tactoid. The peaks resulting from step 2 and step 3, above

223   375 °C, come from decomposition of *intercalated* surfactant molecules.[29] Moreover, we interpret

224   the higher decomposition temperature for the intercalated molecules to be caused by the fact that

225   they are a key part of the clay structure, serving as counterbalancing ions. Since the charge

226   balance must stay intact, these molecules can only exit the clay galleries by degrading during

227   several steps, forming H^+ ions.[15] The adsorbed molecules, on the other hand, may be loosely

228   bound to the surface of the clay by Van der Waals interactions between nonpolar tail groups of

229   CTAB. Furthermore the decomposition products of the intercalated molecules need to diffuse

230   through an extended path along the gallery to exit. Org-Fh releases the intercalated molecules at

231   a higher temperature than the other three organoclays (the peaks from step 2 and step 3 are

232   shifted to higher temperatures). We believe the reason for this is that the higher surface charge of

233   Fh shifts the equilibrium for degradation of CTAB to higher temperatures. On the other hand, the

234   DTGA-peak at around 770 °C for org-Lp, marked with an asterisk (*), is due to dehydroxylation

235   of the silicate structure.[29]

236   The relative mass losses during step 1 (adsorbed species), and subsequently during step 2-3

237   (intercalated species), are presented in Figure 2c and Table 2. From the figure, if org-Lp is not

238   taken into account, it seems that the ratio of adsorbed and intercalated surfactant molecules is

239   strongly correlated with the amount of surface charge present in each clay. The reason why org-

240   Lp shows a much higher value compared to org-HT, although the CEC is almost identical, may

241   be explained by the better dispersion of Lp during the surface treatment, which increases the

242   effective area for the surfactant to be attached.

243
244   **Figure 2.** (a) TGA-traces of the four organoclays, (b) The corresponding DTGA-traces. (c) Mass

245   fraction of adsorbed and intercalated surfactant as a function of CEC.

3.2   Analysis of nanocomposites

3.2.1   WAXS: d-spacing

248   The WAXS-curves of the four different nanocomposites are shown in Figure 3. It is evident

249   that the organoclays did not exfoliate completely during PS-polymerization because distinct

13

250 peaks from 00*l* reflections are still present. The existence of higher order reflections indicates

251 larger and more regular stacking domains in the nanocomposites compared to the organically

252 modified clays alone.[30] Furthermore, the nanocomposites were semi-transparent when inspected

253 in an optical microscope (see Figure S1 in the supporting information), which indicates that the

254 stacked silicate layers form assemblies large enough to scatter visible light.

255 Figure 4 shows high-resolution TEM-micrographs of Laponite (a) and Hectorite (b) clay

256 particles, respectively. The Laponite platelets are well dispersed in the matrix and no large

257 aggregates are observed. Hectorite, on the other hand, displays small 15-20 nm thick tactoids

258 arranged into larger agglomerates. These results are in good agreement with the WAXS results
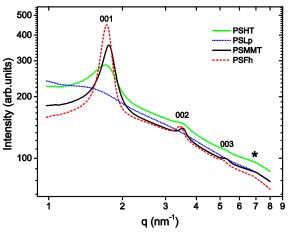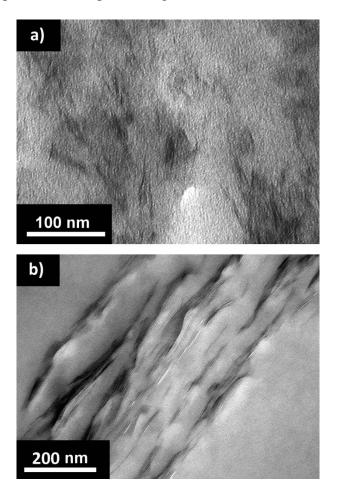
259 discussed later.

260
261 **Figure 3.** WAXS-curves of the four nanocomposites. 00*l*-reflections are labeled. The broad peak

262 at the end of the diffractogram (labeled with *) originates from the amorphous halo of the PS

263 matrix.

264 All four nanocomposite samples show a larger d_{001}-spacing compared to pure organoclays (see

265 Table 2 and Table 3 later) due to intercalation of PS chains between the silicate layers, and it

266 seems that they reach a common value between 3.6 and 4.0 nm. Similar basal spacings in PS-

267   clay nanocomposites have been reported earlier,[10,17,31,32] indicating that the present values

268   produce the optimum space for a compact arrangement of PS chains between silicate sheets.

269
270

271   **Figure 4.** High-resolution TEM micrographs of clay in two nanocomposites. (a) shows well-

272   dispersed Laponite platelets in the PSLp sample, while (b) shows larger stacking structures of

273   Hectorite platelets in the PSHT sample.

274   ### 3.2.2 WAXS: particle/tactoid size

275   The Bragg peaks of the nanocomposites in Figure 3 are broadened beyond the instrumental

276   resolution. The additional contribution from the sample to the peak widths may be obtained by

277   describing each peak by a pseudo-Voigt function, which has two components. One Gaussian

278   component, which counts for the instrumental peak width, and one Lorentzian which counts for

15

279   the broadening due to size/strain effects. A more detailed explanation of the peak fitting

280   procedure is given in the supporting information. The average number of platelets in each tactoid

281   was calculated from the particle/tactoid size which was found using both the Scherrer equation,[33]

282   and a Williamson-Hall analysis.[34] The results for both organoclays and nanocomposites are

283   given in Table 3.

284   **Table 3.** Average basal spacing in the nanocomposites and the number of platelets, N, in the

285   tactoids. The standard deviation in N is ± 1.

Clay type	d_{001}-spacing in nanocomposite (nm)	Number of platelets (N)		
		organoclay	Nanocomposites	
		Scherrer	Scherrer	Williamson-Hall
HT	3.7	7	7	4
Lp	4.0	6	4	-
MMT	3.6	9	15	13
Fh	3.7	8	19	121

286

287   Comparing the values of N for the nanocomposites it is clear that the Scherrer equation

288   underestimates the strain broadening and may lead to apparently larger particle sizes. This is

289   particularly true for PSFh where there is a large discrepancy between the two methods, which

290   originates from the higher strain in this sample compared to PSMMT and PSHT (PSFh shows a

291   steeper slope in Figure S3 in the supplementary information). Except for PSFh, however, the

292   variation of N between the two methods is close to the level of uncertainty, and hence we can

293   assume the values obtained for the organoclays, where only the Scherrer equation could be used,

294   to be valid. Moreover, Uthirakumar et al.[35] prepared PSMMT samples which contained 10-20

295   nm thick MMT-tactoids (with $N\sim6$), a value close to ours. The reason why PSFh displays such a

296   large strain is not obvious, but it may originate from the volume contraction of around 10 %

297   when styrene polymerizes. The large size of the Fh-tactoids can make it difficult to release the

298   stress induced by the shrinking matrix. Another cause may be that org-Fh originally has more

299   disorder in the stacking due to uneven charge distribution between layers.[13]

300   Again it was observed that the surface charge of the clays influences the nanocomposites to a

301   high degree, holding the silicate layers together and increasing the number of platelets in each

302   stack as the surface charge increases. On the other hand, the N values for the four different

303   organoclays in powdered form (no polymer present) are quite similar. A possible reason for this,

304   and also why their tactoids are quite small compared to pure clays, is that the organoclays

305   crystallize nearly instantaneously from single platelets in suspension during the surface

306   treatment. As a comparison, the nominal value for unmodified Na-Fh is between 75 and 100
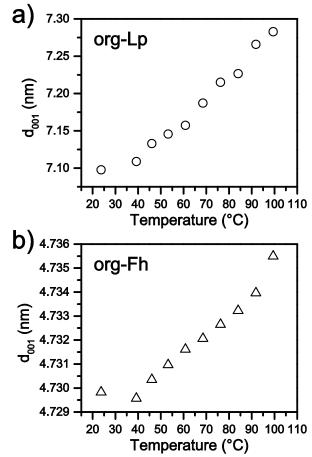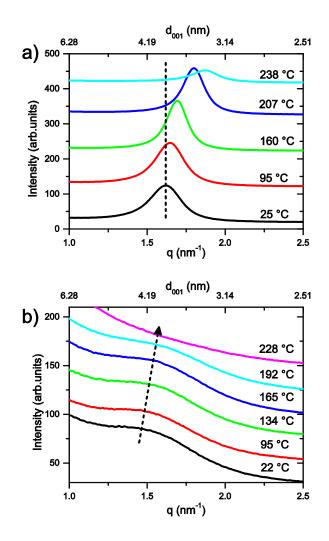
307   platelets in each tactoid.[30]

Figure 5. d_{001}-spacing of org-Lp and org-Fh dispersed in styrene as a function of temperature.

The increase in N in nanocomposites compared to organoclay samples for the Fh- and MMT-systems indicates that the organoclays dissolve to some degree in the styrene monomer, before assembling into larger tactoids. *In situ* WAXS of styrene-clay dispersions showed that when org-Lp was dispersed at room temperature, the d_{001}-spacing increased from 1.5 nm in powdered form up to 7.1 nm when dispersed, while org-Fh increased from 3.1 up to 4.7 nm. Continuous heating up to 100 °C induced a minor additional increase in d-spacing (see Figure 5). The swelled structures and particularly the large increase displayed by org-Lp may help dispersing the clay tactoids through exfoliation. This study also suggests that a low to moderate surface charge could lower the barrier for exfoliation by allowing large d-spacings during polymerization.

18

319   *In situ* heating WAXS-studies up to 250 °C, of PSFh and PSLp, presented in Figure 6, showed

320   noticeable changes in both nanocomposites. The d_{001}-spacing of PSFh (Figure 6a) shrinks during

321   heating because intercalated PS chains are slowly dissolved in the surrounding matrix. The

322   spacing converges towards the value of the organoclay of 3.1 nm, before the sample melts

323   completely. In the melted state the clay structure collapses further due to the release of the

324   remaining PS chains and intercalated surfactant molecules. The spacing of PSLp (Figure 6b), on

325   the other hand, decreases only slightly from 4.1 to 3.9 nm before the 001-reflection disappears

326   completely, indicating full exfoliation of the clay tactoids. Scanning several points in the heat-

327   treated part of the sample after cooling did not reveal any Bragg reflection, meaning that the clay

328   remained mostly exfoliated. This result seems to point out that low-CEC nanocomposites

329   through *in situ* polymerization, and post heating up to 250 °C, may produce well exfoliated clay

330   structures. These findings again suggest a correlation between the surface charge of the clays and

331   the behavior of their respective nanocomposites, showing exfoliation to a higher degree for clay

332   tactoids carrying lower surface charge.

Figure 6. WAXS-curves around the 001-reflection of PSFh (a) and PSLp (b) nanocomposites during heating. Temperatures are indicated next to each curve, and the curves are shifted along the y-axis to make the changes more visible.

3.2.3 Thermal behavior

Figure 7a shows TGA-traces from decomposition of the four different nanocomposites together with a curve of pure PS. All samples have a small mass loss between 200-375 °C, in contrast to the pure polymer which is stable in this temperature range. This loss is most likely due to small amounts of unreacted monomer and surfactant molecules in the composites. The lowest point of the DTGA curves shows the temperature at maximum decomposition rate, and

343 the average of several values for each sample is listed in the inset of Figure 7b. With as little as

344 3.2 wt.% of inorganic filler added, the decomposition temperature is increased for all four

345 nanocomposites. The largest improvement compared to pure PS is seen for the natural HT-clay

346 with a 26 °C higher temperature at maximum decomposition rate. The synthetic Lp-clay and the

347 natural MMT-clay have similar improvements with 21 and 20 °C respectively, which are

348 comparable to MMT-clay values of PSMMT given in a report by Gilman et al.[36] The smallest

349 improvement (12 °C) is found in the synthetic Fluorohectorite clay (Fh), as Gilman et al. also

350 identified when comparing the flame retardant properties of PSMMT and PSFh

351 nanocomposites.[1] This trend also follows the differences in surface charge between the four

352 clays, showing higher decomposition temperatures for the lower CEC values.

353 The higher degradation temperature of polymer-clay nanocomposites compared to pure

354 polymers is related to the superior insulator and mass transport barrier for the volatile products

355 generated during decomposition. A more tortuous path inside the nanocomposites is beneficial

356 for the thermal stability of the material. Based on the models by Bharadadwaj,[37] the tortuosity is

357 increased when well dispersed and large aspect ratio platelets are present in the system, whereas

358 a large stacking number or aggregations produce the opposite effect. This model explains

359 qualitatively our results, dependent on the clay type. Lp-platelets have lower surface charge and

360 a better dispersed morphology, but their aspect ratio is lower than for MMT-platelets. A similar

361 degradation temperature is then obtained. Fh-platelets are larger than the other clays but their

362 surface charge is too high to promote exfoliation and present larger stacking structures. HT-

363 platelets, on the other hand, have both larger area than Lp and a slightly lower surface charge

364 which facilitates exfoliation. These factors turn HT into a better candidate than the other three

365 clays as filler for improving the high-temperature resilience of PS based nanocomposites.
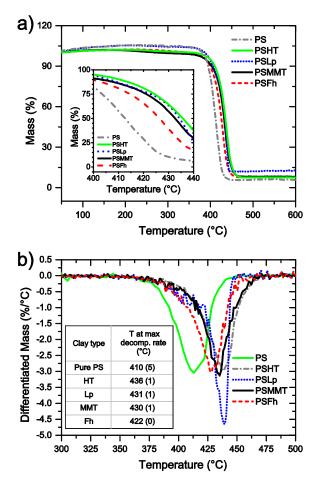
Figure 7. (a) TGA-traces of pure PS and PS-clay nanocomposites. Inset shows a zoomed-in view of the steep drop between 400 and 440 °C. (b) The corresponding DTGA-traces. The inset shows a table with the average decomposition temperatures at maximum decomposition rate. 3σ standard deviation is given in parenthesis.

4   Conclusions

In this work a series of polystyrene-organoclay nanocomposites with different clay surface charge were prepared via in-situ polymerization. Their structure and thermal properties were explored using various experimental techniques. WAXS measurements showed that the resulting nanocomposites were in all cases a mix of intercalated and exfoliated silicate layers. However,

PSLp presented a good dispersion of the platelets, and this was further improved after thermal treatment up to 250 °C.

The intrinsic surface charge of the clays was found to play an important role in the uptake of surfactant molecules and in the dispersion of clay platelets in the PS matrix. A larger surface charge facilitated enhanced intercalation of CTAB, as well as showing an almost linear increase in the number of platelets in each tactoid in both organoclays and nanocomposites. A lower surface charge allowed for increased dispersions for Hectorite and Laponite clay, compared to Montmorillonite and Fluorohectorite, which ultimately resulted in better thermal properties for the former two.

5 Acknowledgements

Supporting Information Available: Picture of the polymerized nanocomposites (Fig. S1). Mass fraction of surfactant in org-clays (Fig. S2). Detailed procedure for performing peak analysis of WAXS data, including fittings of the 00l peaks (Fig. S3) and peak widths (Fig S4), as a function of q. This material is available free of charge via the Internet at http://pubs.acs.org.

6 References

(1) Gilman, J. W.; Jackson, C. L.; Morgan, A. B.; Harris, R.; Manias, E.; Giannelis, E. P.; Wuthenow, M.; Hilton, D.; Phillips, S. H. Flammability properties of polymer - Layered-silicate

397   nanocomposites. Polypropylene and polystyrene nanocomposites. Chem. Mater. 2000, 12, 1866-

398   1873.

399   (2) Zhu, J.; Wilkie, C. A. Thermal and fire studies on polystyrene-clay nanocomposites.

400   Polym. Int. 2000, 49, 1158-1163.

401   (3) Kojima, Y.; Usuki, A.; Kawasumi, M.; Okada, A.; Fukushima, Y.; Kurauchi, T.;

402   Kamigaito, O. Mechanical properties of nylon 6-clay hybrid. J. Mater. Res. 1993, 8, 1185-1189.

403   (4) He, J.; Shen, Y.; Evans, D. G. A nanocomposite structure based on modified MCM-48 and

404   polystyrene. Microporous Mesoporous Mater. 2008, 109, 73-83.

405   (5) Haraguchi, K.; Takehisa, T. Nanocomposite hydrogels: A unique organic-inorganic

406   network structure with extraordinary mechanical, optical, and swelling/de-swelling properties.

407   Adv. Mater. 2002, 14, 1120-1124.

408   (6) Utracki, L. A. Clay-Containing Polymeric Nanocomposites; Smithers Rapra Technology:

409   Shrewsbury, U.K., 2004; Vol. 1.

410   (7) Usuki, A.; Kojima, Y.; Kawasumi, M.; Okada, A.; Fukushima, Y.; Kurauchi, T.;

411   Kamigaito, O. Synthesis of nylon 6-clay hybrid. J. Mater. Res. 1993, 8, 1179-1184.

412   (8) Okada, A.; Usuki, A. Twenty years of polymer-clay nanocomposites. Macromol. Mater.

413   Eng. 2006, 291, 1449-1476.

414   (9) Hasegawa, N.; Kawasumi, M.; Kato, M.; Usuki, A.; Okada, A. Preparation and mechanical

415   properties of polypropylene-clay hybrids using a maleic anhydride-modified polypropylene

416   oligomer. J. Appl. Polym. Sci. 1998, 67, 87-92.

417   (10)   Hasegawa, N.; Okamoto, H.; Kawasumi, M.; Usuki, A. Preparation and mechanical

418   properties of polystyrene-clay hybrids. J. Appl. Polym. Sci. 1999, 74, 3359-3364.

419   (11)   Panwar, A.; Choudhary, V.; Sharma, D. K. A review: polystyrene/clay nanocomposites.

420   J. Reinf. Plast. Compos. 2011, 30, 446-459.

421   (12)   Vaia, R. A.; Ishii, H.; Giannelis, E. P. Synthesis and properties of 2-dimensional

422   nanostructures by direct intercalation of polymer melts in layered silicates. Chem. Mater. 1993,

423   5, 1694-1696.

424   (13)   Alexandre, M.; Dubois, P. Polymer-layered silicate nanocomposites: preparation,

425   properties and uses of a new class of materials. Mater. Sci. Eng., R 2000, 28, 1-63.

426   (14)   Fu, X.; Qutubuddin, S. Synthesis of polystyrene-clay nanocomposites. Mater. Lett.

427   2000, 42, 12-15.

428   (15)   Zhu, J.; Morgan, A. B.; Lamelas, F. J.; Wilkie, C. A. Fire properties of polystyrene-clay

429   nanocomposites. Chem. Mater. 2001, 13, 3774-3780.

430   (16)   Kaviratna, P. D.; Pinnavaia, T. J.; Schroeder, P. A. Dielectric properties of smectite

431   clays. J. Phys. Chem. Solids 1996, 57, 1897-1906.

432   (17)   Mitchell, C. A.; Krishnamoorti, R. Rheological properties of diblock copolymer/layered

433   silicate nanocomposites. J. Polym. Sci., Part B: Polym. Phys. 2002, 40, 1434-1443.

434   (18)   Burmistr, M. V.; Sukhyy, K. M.; Shilov, V. V.; Pissis, P.; Spanoudaki, A.; Sukha, I. V.;

435   Tomilo, V. I.; Gomza, Y. P. Synthesis, structure, thermal and mechanical properties of

436   nanocomposites based on linear polymers and layered silicates modified by polymeric

437   quaternary ammonium salts (ionenes). Polymer 2005, 46, 12226-12232.

438   (19)   Sun, Q. H.; Deng, Y. L.; Wang, Z. L. Synthesis and characterization of polystyrene-

439   encapsulated laponite composites via miniemulsion polymerization. Macromol. Mater. Eng.

440   2004, 289, 288-295.

441   (20)   Zhu, J.; Uhl, F. M.; Morgan, A. B.; Wilkie, C. A. Studies on the mechanism by which

442   the formation of nanocomposites enhances thermal stability. Chem. Mater. 2001, 13, 4649-4654.

443   (21)   Bakk, A.; Fossum, J. O.; da Silva, G. J.; Adland, H. M.; Mikkelsen, A.; Elgsaeter, A.

444   Viscosity and transient electric birefringence study of clay colloidal aggregation. Phys. Rev. E

445   2002, 65, 9.

446   (22)   Chen, B. Q.; Evans, J. R. G. Thermoplastic starch-clay nanocomposites and their

447   characteristics. Carbohydr. Polym. 2005, 61, 455-463.

448   (23)   Moncada, E.; Quijada, R.; Lieberwirth, I.; Yazdani-Pedram, M. Use of PP grafted with

449   itaconic acid as a new compatibilizer for PP/clay nanocomposites. Macromol. Chem. Phys. 2006,

450   207, 1376-1386.

451   (24)   The Clay Minerals Society; Vol. 2013.

452   (25)   Boylu, F.; Hojiyev, R.; Ersever, G.; Ulcay, Y.; Celik, M. S. Production of Ultrapure

453   Bentonite Clays through Centrifugation Techniques. Sep. Sci. Technol. 2012, 47, 842-849.

454   (26)   Labrador, A. L.; Cerenius, Y.; Svensson, S.; Theodor, K.; Plivelic, T. S. The yellow

455   mini-hutch for SAXS experiments at MAX IV Laboratory. J. Phys.: Conf. Ser. 2013, 425,

456   072019.

457   (27)   Hammersley, A. P.; Svensson, S. O.; Hanfland, M.; Fitch, A. N.; Hausermann, D. Two-

458   dimensional detector software: From real detector to idealised image or two-theta scan. High

459   Pressure Res. 1996, 14, 235-248.

460   (28)   Laird, D. A. Influence of layer charge on swelling of smectites. Appl. Clay Sci. 2006,

461   34, 74-87.

462   (29)   Wang, B. X.; Zhou, M.; Rozynek, Z.; Fossum, J. O. Electrorheological properties of

463   organically modified nanolayered laponite: influence of intercalation, adsorption and wettability.

464   J. Mater. Chem. 2009, 19, 1816-1828.

465   (30)   da Silva, G. J.; Fossum, J. O.; DiMasi, E.; Maloy, K. J.; Lutnaes, S. B. Synchrotron x-

466   ray scattering studies of water intercalation in a layered synthetic silicate. Phys. Rev. E 2002, 66.

467   (31)   Arora, A.; Choudhary, V.; Sharma, D. K. Effect of clay content and clay/surfactant on

468   the mechanical, thermal and barrier properties of polystyrene/organoclay nanocomposites.

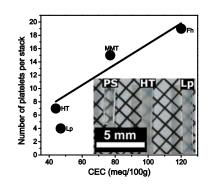469   Journal of Polymer Research 2011, 18, 843-857.

470   (32)   Qi, R.; Jin, X.; Huang, S. Synthesis and Characteristics of Polystyrene-Clay

471   Nanocomposites via In Situ Intercalative Polymerization in a Direct Current Electric Field. J.

472   Appl. Polym. Sci. 2010, 115, 2723-2727.

473   (33)   Patterson, A. L. The Scherrer formula for x-ray particle size determination. Physical

474   Review 1939, 56, 978-982.

475   (34)   Williamson, G. K.; Hall, W. H. X-ray line broadening from filed aluminium and

476   wolfram. Acta Metall. 1953, 1, 22-31.

477   (35)   Uthirakumar, P.; Nahm, K. S.; Hahn, Y. B.; Lee, Y. S. Preparation of

478   polystyrene/montmorillonite nanocomposites using a new radical initiator-montmorillonite

479   hybrid via in situ intercalative polymerization. Eur. Polym. J. 2004, 40, 2437-2444.

480   (36)   Gilman, J. W.; Kashiwagi, T.; Morgan, A. B.; Harris, R.; Brassell, L.; Vanlandingham,

481   M.; Jackson, C. L. Flammability of polymer clay nanocomposites consortium: Year One Annual

482   Report, US Dept. Commerce, Technology Administration, National Institute of Standards and

483   Technology, 2000.

484   (37)   Bharadwaj, R. K. Modeling the barrier properties of polymer-layered silicate

485   nanocomposites. Macromolecules 2001, 34, 9189-9192.

486

487

488

489   TOC Graphic

490

The effect of clay surface charge on the emerging properties of Polystyrene-organoclay nanocomposites

Henrik Mauroy*[a,b], Tomás S. Plivelic[c] ,Elisabeth L. Hansen[d], Jon Otto Fossum[d], Geir Helgesen[a,b] and Kenneth D. Knudsen*[a,d]

[a]Physics department, Institute for Energy Technology, P.O. Box 40, N-2027 Kjeller, Norway

[b]Department of Physics, University of Oslo, N-0316 Oslo, Norway

[c]MAX IV Laboratory, Lund University, P.O. Box 118, SE-221 00 Lund, Sweden

[d]Department of Physics, Norwegian University of Science and Technology, Hoegskoleringen 5, N-7491 Trondheim, Norway

*E-mail: Kenneth D. Knudsen: kenneth.knudsen@ife.no; Henrik Mauroy: henrik.mauroy@ife.no

Supporting information

1 Picture of the finished nanocomposites

The polymerized nanocomposites are displayed in Figure S1 together with a pure polystyrene (PS) sample. All samples, except PS-Fluorohectorite (Fh) were semitransparent.
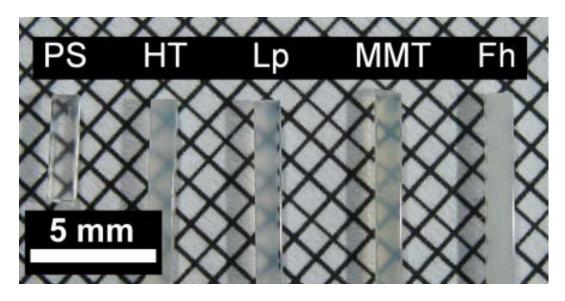
Figure S1. Picture of the finished nanocomposites. From left: pure PS, PS-Hectorite (HT), PS-Laponite (Lp), PS-Montmorillonite (MMT) and PS-Fluorohectorite (Fh).

2 Mass fraction of surfactant in org-clays

The total amount of surfactant intercalated and adsorbed by the clays during surface treatment was determined with thermogravimetric analysis (TGA). The results indicated an almost linear correlation between clay surface charge and the total uptake of surfactant as is shown in Figure S2.
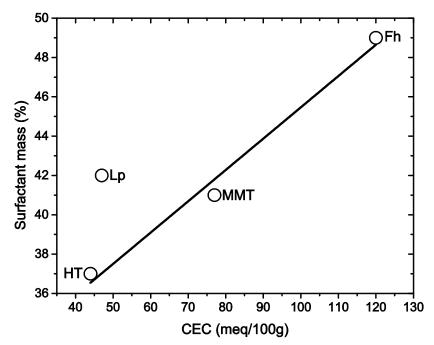
Figure S2. Mass fraction of surfactant in org-clays as a function of CEC.

3 Peak fitting of x-ray data

3.1 Introduction

A detailed description of the determination of the thickness of the clay tactoids in the nanocomposites is presented below. The 00*l* reflections for both the organoclays and organoclays inside the nanocomposites are broadened beyond the instrumental resolution. The additional contribution from the sample to the peak widths can be obtained by deconvoluting the scattered intensity *I(q)=C(q)Φ(q)*. The *C* parameter is related to the scattering setup and polarization factors, and can be approximated by a constant value in the region around each 00*l* peak since it varies slowly with *q* compared to the peak widths.[1] After subtracting a polynomial function for the background contribution around each peak, and normalizing the intensity to 1, the 00*l* reflections for the organoclays and the nanocomposites were fitted with a pseudo-Voigt function

$$\Phi(q) = \frac{2\eta}{\pi\Gamma(1 + 4(q - q_c)^2/\Gamma^2)} + 2\frac{1 - \eta}{\Gamma}\left(\frac{ln2}{\pi}\right)^{1/2} e^{-4ln2(q-q_c)^2/\Gamma^2} \tag{1}$$

that approximates the peak profile as a linear combination of a Gaussian and a Lorentzian component.[2] q_c is the refined center of the peak, Γ is the measured width at half maximum (FWHM) and η is a mixing parameter between zero and one that determines the extent of the Lorentzian contribution. Γ and η can be expressed as a function of the Gaussian, Γ_G, and Lorentzian, Γ_L, width contribution, which are directly connected to Γ and η with two polynomial expressions[2],

$$\Gamma = \Gamma_G^5 + 2.6927\Gamma_G^4\Gamma_L + 2.4284\Gamma_G^3\Gamma_L^2 + 4.471\Gamma_G^2\Gamma_L^3 + 0.0784\Gamma_G\Gamma_L^4 + \Gamma_L^5 \tag{2}$$

$$\eta = 1.36603\frac{\Gamma_L}{\Gamma} - 0.47719\frac{\Gamma_L^2}{\Gamma^2} + 0.11116\frac{\Gamma_L^3}{\Gamma^3} \tag{3}$$

In order to determine the instrumental peak broadening, the 111 reflection from a silicon powder standard was fitted with eq. 1. Normally the instrumental broadening is attributed to the Gaussian component alone. However, we here allow also for a minor contribution from a Lorentzian component. The fit resulted in $\Gamma_G = 0.09663$ nm^{-1} and $\Gamma_L = 0.03967$ nm^{-1}. $\Gamma_G = 0.09663$ nm^{-1} was thus set as a locked parameter in eq. 1 in the later fitting procedure, and only Γ_L and q_c were refined. The instrumental contribution to Γ_L was later subtracted from the

sample's Γ_L. Figure S3 shows the results of the fitting for some of the samples, and also examples of the Gaussian and Lorentzian contributions.
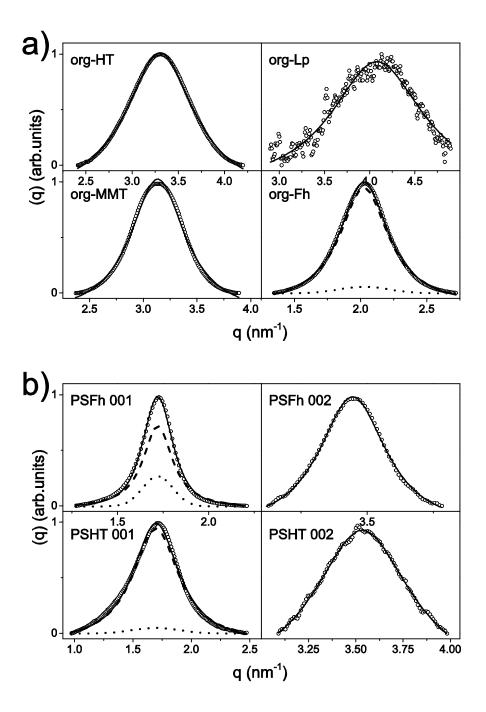

Figure S3. Peak fitting of the a) organoclays and b) the 001 and 002 reflections from PSFh and PSHT. The open symbols are the experimental data, and the continuous lines are the fits. The

dotted and dashed lines in the panel for org-Fh and the panels for the 001 peaks show the Gaussian and Lorentzian contributions, respectively.

3.2 Williamson-Hall analysis

The Lorentzian component of the FWHM is connected with the effect of both the particle size and strain on the silicate layer stacking.[3] The average thickness of each clay tactoid, and thus the number of platelets they contain, can therefore be determined from a Williamson-Hall[3] plot according to the following relations:[1]

$$\Gamma_L = \frac{2\pi}{Nd} + \xi q \qquad (4)$$

where N is the number of platelets in a clay stack, d is the d_{00l}-spacing and ξ is the strain. The slope of the straight line gives the strain and its intercept at $q = 0$ estimates the thickness.

Figure S4 shows the plots of the widths Γ_L versus peak positions for PSFh, PSMMT and PSHT. The calculated values for N and the strain ξ are shown as insets. PSLp could not be analyzed with this method because it did not show any higher order reflections. An absence of higher order reflections was also the case for the organoclay-powders, except org-Fh which showed a weak 002 reflection.
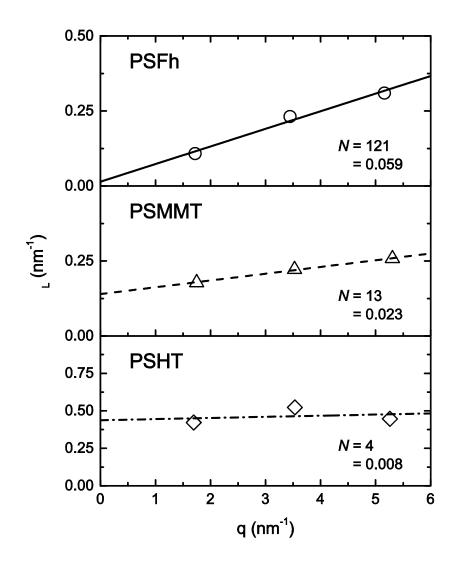
Figure S4. Williamson-Hall plot for PSFh, PSMMT and PSHT. The straight lines are fitted to the function in eq. 4, and the calculated values for N and the strain ξ are shown as insets.

3.3 Scherrer equation

Another method to estimate the average number of platelets in the tactoids is the Scherrer equation:[4]

$$Nd = \frac{K \cdot \lambda}{\Delta\theta_L \cdot cos\theta} \tag{3}$$

where d is the d_{001}-spacing, K (~0.9) is a numerical constant, $\Delta\theta_L$ is the Lorentzian component of the FWHM measured in radians and 2θ the Bragg angle. The average number of platelets in each tactoid for both the organoclay-powders and the nanocomposites, based on eq. (2) and (3), are presented in Table 3 of the manuscript.

4 References

(1) da Silva, G. J.; Fossum, J. O.; DiMasi, E.; Maloy, K. J.; Lutnaes, S. B. Synchrotron X-Ray Scattering Studies of Water Intercalation in a Layered Synthetic Silicate. *Phys. Rev. E* **2002**, 66.

(2) Thompson, P.; Cox, D. E.; Hastings, J. B. Rietveld Refinement of Debye-Scherrer Synchrotron X-Ray Data from Al2o3. *J. Appl. Crystallogr.* **1987**, 20, 79-83.

(3) Williamson, G. K.; Hall, W. H. X-Ray Line Broadening from Filed Aluminium and Wolfram. *Acta Metall.* **1953**, 1, 22-31.

(4) Patterson, A. L. The Scherrer Formula for X-Ray Particle Size Determination. *Physical Review* **1939**, 56, 978-982.